

Numerical Determination of Flow Corrective Inserts for Granular Materials in Conical Hoppers*

PIERRE-ALAIN GREMAUD†, DAVID G. SCHAEFFER‡, AND MICHAEL SHEARER†

Abstract. The flow of granular materials in hoppers is studied. In industrial applications, inserts of various size and shape are often used to improve the flow properties and get rid of undesirable effects such as material sticking to the walls, funnel flow, arching, etc. We study the case of inverted conical inserts in conical hoppers. In spite of the complexity of the phenomenon as observed in practice, existing methods assume in general a radial structure of the stress and velocity fields. A new numerical approach to the problem of designing “optimal” inserts is proposed and tested. It allows for non purely radial solutions. The new criterion is found to be more stringent than criteria based on fully radial constructions. Comparisons with experiments as well as general comments about the overall approach are offered.

Key words. granular flow, boundary value problem, yield condition, flow rule

AMS(MOS) subject classifications. 65L10, 73E05, 35Q72

1. Introduction. In the 1960’s, Jenike [2] proposed a special solution of steady state equations describing the flow of a cohesionless granular material in a conical hopper. This solution, the so-called *radial flow solution* is the basis for much work on the design of industrial hoppers for the handling of many different kinds of granular materials [3]. Much remains to be understood about the radial solution, especially its stability [7, 8], and the importance of the simplifying assumptions employed by Jenike [9].

In this paper, we begin an analysis of a related but more intricate problem of industrial importance, using Jenike’s approach to the equations of motion. The problem addressed here is that of the flow in the space between an inverted conical insert and the hopper wall. More specifically, we consider three dimensional axisymmetric flow between a small inverted cone (the insert) and a large cone (the hopper) that have the same axis of rotation, see Figure 1.1. Conical inserts have been studied and used as a means to improve flow characteristics in hoppers, especially those for which the radial solution appears not to be valid, and the flow is instead *funnel flow*, in which material flows down a central funnel, leaving a stagnant region adjacent to the hopper wall. Incidentally, the transition between mass flow, in which all the material is mobilized in a steady smooth flow, and funnel flow is thought to be associated with the breakdown of the radial flow solution as the material or hopper parameters are changed. Indeed, this association has been the basis for much of the design of mass-flow hoppers.

Consider the flow between the insert and the hopper as shown in Figure 1.1, with toroidal coordinates (r, θ, ϕ) , in which ϕ is the angle of rotation about the axis, and r, θ are plane polar coordinates in the plane $\phi = \text{const}$, centered at the point at which the insert would intersect the hopper if the insert were continued as shown by the

* The first author was supported by the Army Research Office through grants DAAH04-95-1-0419 and DAAH04-96-1-0097, and by the North Carolina Supercomputing Center. The second author.... The third author was supported by National Science Foundation grant DMS 9504583, and by Army Research Office grant (DAAH0 98 numbers to come).

† Center for Research in Scientific Computation and Department of Mathematics, North Carolina State University, Raleigh, NC 27695-8205.

‡ Department of Mathematics, Duke University, Durham, NC 27706.

dashed line in Figure 1.1. Of course, the flow in this space will be influenced by the flow above the insert, and possibly by the flow below the insert. Nonetheless, we seek special solutions that may describe the flow in a region between the insert and the hopper, just as the radial flow solution in a hopper provides an accurate description of flow even in circumstances in which the flow above the hopper is decidedly not radial. The thinking here is that there may be a small transition region near the level (i.e., values of r) of the vertex of the insert in which the flow adjusts to the special solution we seek. The special solution can then be used to understand how the insert mobilizes material on the hopper wall, leading to a more refined design of hopper inserts.

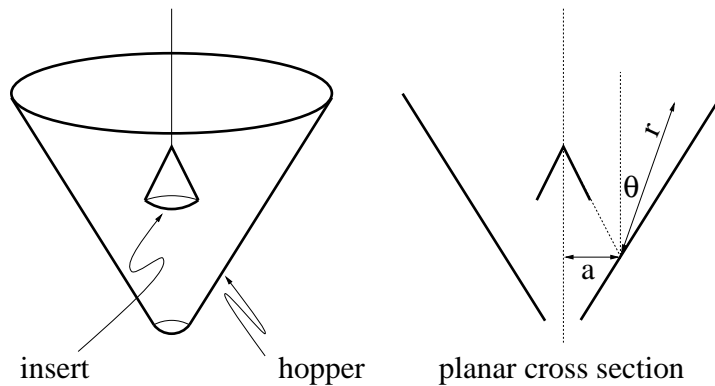


FIGURE 1.1. *Conical hopper with an inverted cone insert.*

The literature on the flow of granular materials around obstacles in general, and on the subject of rigid inserts in particular is rather scarce, and mostly empirical. To the authors' knowledge, the earliest work is by Johanson [5] where a design procedure for conical inserts is laid out. As reported in [5], the flow may be thought of as being roughly planar and radial, at least away from the vertex of the insert. The intuition here is that locally the space between the hopper wall and the insert is nearly a wedge, (i.e., with slightly curved walls), so that the curvature of the hopper and of the insert should represent a higher order correction to a planar radial solution, in which the origin is $r = 0, \phi = \text{constant}$. We explore this intuitive idea by writing the equations of motion in the coordinates of Figure 1.1, and seeking solutions as an asymptotic series in powers of r/a , much as Jenike's solution employs scaling of the dependent variables of stress and velocity by powers of R , the distance of a material point from the vertex of the hopper.

With this new approach, we extract the radial solution as the leading order term in the expansion. We then formulate equations for the next order terms, representing a correction to the plane radial solution. This correction is hoped to partially alleviate some of the obvious shortcomings [10, p.327] of the purely radial approach of [5]. The equations (at both orders) are solved numerically for representative physical parameters. The outline of the paper is as follows. In Section 2, the equations of motion are derived and discussed. Section 3 is devoted to the construction of the above mentioned expansion. Numerical experiments are discussed in Section 4. Finally, conclusions are offered in Section 5.

2. Equations of Motion. We consider steady incompressible flow in which the

particles have no motion in the axial (or φ) direction. Then the dependent variables reduce to four components of stress and two of velocity:

$$T = \begin{pmatrix} T_{rr} & T_{r\vartheta} & 0 \\ T_{r\vartheta} & T_{\vartheta\vartheta} & 0 \\ 0 & 0 & T_{\varphi\varphi} \end{pmatrix} \quad v = \begin{pmatrix} v_r \\ v_\vartheta \\ 0 \end{pmatrix}. \quad (2.1)$$

The equations of motion are

$$\nabla \cdot T = \rho g, \quad (2.2)$$

in which ρ is the density, taken to be constant, and the vector g is the acceleration due to gravity, and

$$\nabla \cdot v = 0, \quad (2.3)$$

Equations (2.2) represent the balance of forces in the material, while equation (2.3) expresses incompressibility. Note that because gravity has no component in the axial direction, T is independent of φ , and given the form (2.1) of the stress tensor T , equations (2.2) reduce to two equations, so that the system (2.2,2.3) consists of three equations in the six unknowns of (2.1).

Added to these equations are constitutive laws. Let $p = \text{tr } T/3$ be the *average stress*, more precisely the average of the principal stresses σ_i , $i = 1, 2, 3$, the eigenvalues of T . Assuming plastic deformation everywhere, we impose the *von Mises yield condition*

$$\sum_{i=1}^3 (\sigma_i - p)^2 = 2 \sin^2 \delta p^2, \quad (2.4)$$

where δ is the angle of internal friction. Finally, we have the *flow rule*, which relates the stress to the deformation through the *strain rate tensor*, defined as

$$V = -\frac{1}{2}(\nabla v + \nabla v^T).$$

The condition of *alignment*, the flow rule used here, is that there exist a scalar $q > 0$ such that

$$V = q(T - pI). \quad (2.5)$$

In particular, since $\nabla \cdot V = \text{tr } V$, and the right hand side of (2.5) has zero trace, the flow rule is consistent with the incompressibility condition (2.3). Equation (2.4) is a single algebraic constraint on the stress, while equation (2.5) reduces to two equations relating the stress and velocity gradients. Thus, equations (2.2–2.5) represent a set of six equations in the six unknowns of (2.1).

In the coordinates of Figure 1.1, the strain rate tensor becomes

$$V = \begin{pmatrix} -\partial_r v_r & (-\frac{1}{r}\partial_\vartheta v_r - \partial_r v_\vartheta + \frac{v_\vartheta}{r})/2 & 0 \\ (-\frac{1}{r}\partial_\vartheta v_r - \partial_r v_\vartheta + \frac{v_\vartheta}{r})/2 & -\frac{1}{r}(\partial_\vartheta v_\vartheta + v_r) & 0 \\ 0 & 0 & -\frac{v_r \sin \vartheta + v_\vartheta \cos \vartheta}{a + r \sin \vartheta} \end{pmatrix},$$

and the six equations are

$$\begin{aligned} \partial_r T_{rr} + \frac{1}{r} \partial_\vartheta T_{r\vartheta} + \left(\frac{1}{r} + \frac{\sin \vartheta}{a + r \sin \vartheta}\right) T_{rr} + \frac{\cos \vartheta}{a + r \sin \vartheta} T_{r\vartheta} \\ - \frac{1}{r} T_{\vartheta\vartheta} - \frac{\sin \vartheta}{a + r \sin \vartheta} T_{\varphi\varphi} = -\rho g \cos \vartheta, \end{aligned} \quad (2.6)$$

$$\partial_r T_{r\vartheta} + \frac{1}{r} \partial_\vartheta T_{\vartheta\vartheta} + \left(\frac{2}{r} + \frac{\sin \vartheta}{a + r \sin \vartheta} \right) T_{r\vartheta} + \frac{\cos \vartheta}{a + r \sin \vartheta} (T_{\vartheta\vartheta} - T_{\varphi\varphi}) = \rho g \sin \vartheta, \quad (2.7)$$

$$(T_{rr} - p)^2 + (T_{\vartheta\vartheta} - p)^2 + (T_{\varphi\varphi} - p)^2 + 2T_{r\vartheta}^2 = 2 \sin^2 \delta p^2, \quad (2.8)$$

$$\frac{\frac{\sin \vartheta}{a + r \sin \vartheta} v_r + \frac{\cos \vartheta}{a + r \sin \vartheta} v_\vartheta}{\frac{1}{r} \partial_\vartheta v_\vartheta + \frac{1}{r} v_r} = \frac{T_{\varphi\varphi} - p}{T_{\vartheta\vartheta} - p}, \quad (2.9)$$

$$\frac{1}{2} \frac{\partial_r v_\vartheta + \frac{1}{r} \partial_\vartheta v_r - \frac{1}{r} v_\vartheta}{\frac{1}{r} \partial_\vartheta v_\vartheta + \frac{1}{r} v_r} = \frac{T_{r\vartheta}}{T_{\vartheta\vartheta} - p}, \quad (2.10)$$

$$\partial_r v_r + \frac{1}{r} \partial_\vartheta v_\vartheta + \left(\frac{1}{r} + \frac{\sin \vartheta}{a + r \sin \vartheta} \right) v_r + \frac{\cos \vartheta}{a + r \sin \vartheta} v_\vartheta = 0. \quad (2.11)$$

Equations (2.6) and (2.7) are the stress equilibrium conditions, while (2.8) is the von Mises yield condition. Equations (2.9) and (2.10) are direct consequences of the flow rule (2.5). Finally, (2.11) is the continuity equation expressing incompressibility.

The above system is completed with the following boundary conditions

$$T_{r\vartheta}(\vartheta_1) = \mu T_{\vartheta\vartheta}(\vartheta_1) \quad T_{r\vartheta}(\vartheta_2) = -\mu T_{\vartheta\vartheta}(\vartheta_2), \quad (2.12)$$

$$v_\vartheta(\vartheta_1) = 0 \quad v_\vartheta(\vartheta_2) = 0. \quad (2.13)$$

Equation (2.12) describes the friction effects on the walls of both the insert ($\vartheta = \vartheta_1$) and the hopper ($\vartheta = \vartheta_2$). For the sake of simplicity, we assume the same coefficient of wall friction μ for both insert and hopper.

3. Expansion for the hopper/insert system. In the case of the hopper/insert problem, there is no similarity solution. For $a \neq 0$, $a \gg r$, see Figure 1.1, we consider instead the following expansion

$$\begin{aligned} T &= rT^0(\vartheta) + r^2T^1(\vartheta) + \dots, \\ v &= \frac{1}{r}v^0(\vartheta) + v^1(\vartheta) + \dots \end{aligned} \quad (3.1)$$

We introduce new Sokolovskii variables to rewrite the first three components of the stress tensor. For $k = 0, 1$, we set

$$\begin{pmatrix} T_{rr}^k(\vartheta) & T_{r\vartheta}^k(\vartheta) \\ T_{r\vartheta}^k(\vartheta) & T_{\vartheta\vartheta}^k(\vartheta) \end{pmatrix} = \sigma^k(\vartheta) \mathbb{I} + \tau^k(\vartheta) \begin{pmatrix} -\cos 2\psi^k(\vartheta) & -\sin 2\psi^k(\vartheta) \\ -\sin 2\psi^k(\vartheta) & \cos 2\psi^k(\vartheta) \end{pmatrix}. \quad (3.2)$$

Relations (3.1) and (3.2) are then substituted in (2.6–2.11), and the coefficients of equal power of r equated. Only terms of order 0 and 1 are considered here. We have found it convenient to work with the following stress variables

$$\sigma^0, \psi^0, w = \tau^1 \cos 2\psi^1, z = \tau^1 \sin 2\psi^1,$$

so that in effect the τ variables from (3.2) are not explicitly present. For the velocity, the variables are

$$v_r^0, v_r^1, v_\vartheta^1.$$

From (2.9), one observes

$$T_{\varphi\varphi}^0 = p^0 = \sigma^0. \quad (3.3)$$

Using (2.8), it then follows that

$$\tau^0 = \sigma^0 \sin \delta \quad (3.4)$$

Using relations (2.6) and (2.7) lead to the system

$$\begin{pmatrix} -\sin \delta \sin 2\psi^0 & -2\sigma^0 \sin \delta \cos 2\psi^0 \\ 1 + \sin \delta \cos 2\psi^0 & -2\sigma^0 \sin \delta \sin 2\psi^0 \end{pmatrix} \begin{pmatrix} \sigma^0 \\ \psi^0 \end{pmatrix}' + \begin{pmatrix} \sigma^0(1 - 3 \sin \delta \cos 2\psi^0) \\ -3\sigma^0 \sin \delta \sin 2\psi^0 \end{pmatrix} = \begin{pmatrix} -\rho g \cos \vartheta \\ \rho g \sin \vartheta \end{pmatrix}, \quad \vartheta \in (\vartheta_1, \vartheta_2). \quad (3.5)$$

The system (3.5) is completed by two boundary conditions

$$T_{r\vartheta}(\vartheta_1) = \mu T_{\vartheta\vartheta}(\vartheta_1) \quad T_{r\vartheta}(\vartheta_2) = -\mu T_{\vartheta\vartheta}(\vartheta_2).$$

The above equations can be solved and yield boundary conditions on ψ^0

$$\psi^0(\vartheta_1) = -\psi_w \quad \psi^0(\vartheta_2) = \psi_w, \quad (3.6)$$

with $\psi_w = \frac{\arctan \mu}{2} + \frac{1}{2} \arcsin\left(\frac{\sin(\arctan \mu)}{\sin \delta}\right) = \frac{1}{2}(\Phi + \arcsin(\frac{\sin \Phi}{\sin \delta}))$ where Φ , $\mu = \tan \Phi$, is the angle of wall friction. Incidentally, the above relation makes sense only if the angle of wall friction Φ is less or equal to the angle of internal friction δ , i.e., $\Phi \leq \delta$, or equivalently, $\mu \leq \tan \delta$. In practice, the roughness of the walls is usually such that the previous condition is comfortably satisfied [7, p.46]. The relationship between ψ_w and (μ, δ) is illustrated in Figure 3.1.

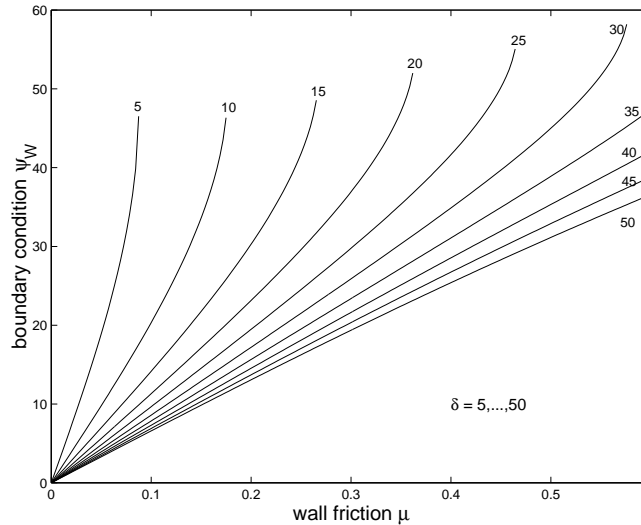


FIGURE 3.1. Dependence of the boundary condition ψ_w with respect to the wall friction μ for various values the angle of internal friction δ .

Note that the above problem (3.5, 3.6), corresponding to the lowest order terms in our expansion, is exactly Jenike's radial solution in the planar case. We now turn to the derivation of the equations for the first order terms. Using (2.9), we get

$$T_{\varphi\varphi}^1 = p^1 + \frac{\sin \vartheta}{a} \sigma^0 \sin \delta \cos 2\psi^0,$$

and thus, by definition of p^1

$$p^1 = \sigma^1 + \frac{\sin \vartheta}{2a} \sigma^0 \sin \delta \cos 2\psi^0. \quad (3.7)$$

This last relation is the first order analog to (3.3). Then, (2.8) leads to

$$\tau^0 \tau^1 \cos 2(\psi^0 - \psi^1) = \sin^2 \delta \sigma^0 p^1,$$

and thus, by (3.4) and (3.7)

$$\tau^1 \cos 2(\psi^0 - \psi^1) = \sin \delta \left(\sigma^1 + \frac{\sin \vartheta}{2a} \sigma^0 \sin \delta \cos 2\psi^0 \right). \quad (3.8)$$

The last equation (3.8) will be regarded as an equation for σ^1 , once ψ^1 and τ^1 have been determined. Equations for ψ^1 and τ^1 are obtained from (2.6) and (2.7), which yield

$$\begin{aligned} (-\tau^1 \sin 2\psi^1)' + 2\sigma^1 - 4\tau^1 \cos 2\psi^1 &= \frac{\sigma^0}{a} \sin \delta \sin(\vartheta + 2\psi^0), \\ (\sigma^1 + \tau^1 \cos 2\psi^1)' - 4\tau^1 \sin 2\psi^1 &= -\frac{\sigma^0}{a} \sin \delta \cos(\vartheta + 2\psi^0). \end{aligned} \quad (3.9)$$

The first order counterpart to the boundary conditions (3.16) is found to be

$$\begin{aligned} -v(\vartheta_1) &= \mu(u(\vartheta_1) + w(\vartheta_1)), \\ v(\vartheta_2) &= \mu(u(\vartheta_2) + w(\vartheta_2)), \end{aligned}$$

where u is determined by

$$u = \frac{1}{\sin \delta} \left(w \cos 2\psi^0 + z \sin 2\psi^0 - \frac{\sin^2 \delta}{2a} \sigma^0 \sin \vartheta \cos 2\psi^0 \right). \quad (3.10)$$

We now turn to the determination of the velocity equations, starting with order 0. At the zero-th order, equation (2.11) reduces to

$$\partial_\vartheta v_\vartheta^0 = 0,$$

and thus, since v_ϑ has to vanish on the boundary

$$v_\vartheta^0 \equiv 0. \quad (3.11)$$

The equation for v_r^0 is obtained from (2.10) which reads here

$$\partial_\vartheta v_r^0 = -2 v_r^0 \tan 2\psi^0. \quad (3.12)$$

No boundary conditions are imposed on v_r^0 . This could be done, for instance, by imposing the withdrawal rate $\rho \int v_r r d\vartheta$.

To obtain the first order equations for the velocities, we first note

$$\frac{T_{r\vartheta}}{T_{\vartheta\vartheta} - p} = \frac{T_{r\vartheta}^0}{T_{\vartheta\vartheta}^0 - p^0} + r \left(\frac{T_{r\vartheta}^1}{T_{\vartheta\vartheta}^0 - p^0} - \frac{T_{r\vartheta}^0 (T_{\vartheta\vartheta}^1 - p^1)}{(T_{\vartheta\vartheta}^0 - p^0)^2} \right) + \dots$$

Equation (2.10) then leads to

$$\partial_\vartheta v_r^1 + 2 \tan 2\psi^0 (\partial_\vartheta v_\vartheta^1 + v_r^1) - v_\vartheta^1 = -\frac{\sin 2\psi^0}{\sigma^0 \sin \delta \cos^2 2\psi^0} \left(2w + \frac{\sin \vartheta}{a} \sigma^0 \sin \delta \cos 2\psi^0 \right) v_r^0. \quad (3.13)$$

On the other hand, (2.11) yields the equation for v_ϑ^1 , which is found to be

$$\partial_\vartheta v_\vartheta^1 + v_r^1 = -\frac{\sin \vartheta}{a} v_r^0. \quad (3.14)$$

The fact that v_ϑ vanishes on the boundary provides the additional conditions necessary to close our system

$$v_\vartheta^1(\vartheta_1) = v_\vartheta^1(\vartheta_2) = 0.$$

For convenience, the equations are rewritten in a more compact form.

$$\begin{pmatrix} A & B & 0 & 0 & 0 & 0 & 0 \\ C & D & 0 & 0 & 0 & 0 & 0 \\ 0 & 0 & 0 & E & 0 & 0 & 0 \\ F & G & H & I & 0 & 0 & 0 \\ 0 & 0 & 0 & 0 & 1 & 0 & 0 \\ 0 & 0 & 0 & 0 & 0 & 1 & J \\ 0 & 0 & 0 & 0 & 0 & 0 & 1 \end{pmatrix} \begin{pmatrix} \sigma^0 \\ \psi^0 \\ w \\ z \\ v_r^0 \\ v_r^1 \\ v_\vartheta^1 \end{pmatrix}' + \begin{pmatrix} K \\ L \\ M \\ N \\ O \\ P \\ Q \end{pmatrix} = \begin{pmatrix} -\rho g \cos \vartheta \\ \rho g \sin \vartheta \\ 0 \\ 0 \\ 0 \\ 0 \\ 0 \end{pmatrix}. \quad (3.15)$$

The above system of ODEs is closed with the following boundary conditions, deriving from (2.12, 2.13)

$$\psi^0(\vartheta_1) = -\psi_w \quad \psi^0(\vartheta_2) = \psi_w, \quad (3.16)$$

$$-v(\vartheta_1) = \mu(\sigma^1(\vartheta_1) + w(\vartheta_1)), \quad v(\vartheta_2) = \mu(\sigma^1(\vartheta_2) + w(\vartheta_2)), \quad (3.17)$$

$$v_\vartheta^1(\vartheta_1) = 0 \quad v_\vartheta^1(\vartheta_2) = 0, \quad (3.18)$$

where the various quantities appearing in (3.15) are described in the Appendix. Note that there are no boundary conditions on σ^0 , w and v_r^1 . Further, (3.15) is in fact well posed, even we have six boundary conditions and seven unknowns, since two boundary conditions were carrying on an eighth variable v_ϑ^0 , which is identically zero.

By examining the structure of the above system, one can see that upon approximation by the series (3.1), the stress equations can be solved both at the zero-th and the first order, independently of the velocity equations (this is not true of the PDE's). We can thus decompose the ODE into three problems of increasing complexity by solving a problem for the zero-th order stress terms first, then by solving for the first order stress terms, and finally by solution for the components of the velocity. With the notation of (3.15), the three corresponding matrices are respectively

$$M_0 = \begin{pmatrix} A & B \\ C & D \end{pmatrix}, \quad M_1 = \begin{pmatrix} A & B & 0 & 0 \\ C & D & 0 & 0 \\ 0 & 0 & 0 & E \\ F & G & H & I \end{pmatrix}, \quad M = \begin{pmatrix} A & B & 0 & 0 & 0 & 0 & 0 \\ C & D & 0 & 0 & 0 & 0 & 0 \\ 0 & 0 & 0 & E & 0 & 0 & 0 \\ F & G & H & I & 0 & 0 & 0 \\ 0 & 0 & 0 & 0 & 1 & 0 & 0 \\ 0 & 0 & 0 & 0 & 0 & 1 & J \\ 0 & 0 & 0 & 0 & 0 & 0 & 1 \end{pmatrix}. \quad (3.19)$$

Again, we stress that only the zero-th order stress terms appear in the equation corresponding to M_0 . Likewise, the M_1 -equation only contains zero and first order stress terms. This fact is used in the next section. Further, we observe that each of the three systems M_0 , M_1 and M is singular under the same condition. Indeed, one easily

checks

$$\begin{aligned}\det M_0 &= 2\sigma^0 \sin \delta (\cos 2\psi^0 + \sin \delta), \\ \det M_1 = \det M &= -2\sigma^0 \sin^2 \delta (\cos 2\psi^0 + \sin \delta)^2.\end{aligned}$$

Therefore, putting aside the particular case $\sigma^0 = 0$ and/or $\sin \delta = 0$, the stress equations are singular if

$$\cos 2\psi^0 + \sin \delta = 0, \quad (3.20)$$

while each of the three velocity equations (3.12–3.14) are singular whenever

$$\psi^0 = \pi/4 = 45^\circ. \quad (3.21)$$

We will use this condition to numerically determine the stagnant part of the flow in the next section.

4. Numerical results. The numerical method is based on the two following main steps

(1) use of a Runge-Kutta-Fehlberg 4(5) method with automatic step size selection for integrating the ODEs (i.e., a 4th order Runge-Kutta where the local truncation error is estimated through a fifth order formula, and is then used for step size selection);

(2) use of an inexact Newton method for solving the nonlinear problems arising from the shooting steps (see below).

As described in the previous section, we have to solve a boundary value problem consisting of seven nonlinear coupled ODEs. Numerically, this is done by solving a sequence of initial value problems where the “missing” initial values are sought so as to satisfy the prescribed boundary conditions, i.e., the so-called shooting method is used.

As is well known, the shooting method can lead to various problems in practice. As an alternative to multiple shooting, the shooting process is done here in several steps, in order to take advantage of the block structure of the system (3.15). The approach is simpler than multiple shooting and works well in the present context.

First, the equation corresponding to M_0 , (3.19.1), is solved for the 0th order stress terms σ^0 and ψ^0 , is solved. The boundary conditions (3.16) are adjusted through shooting on σ . Second, the system corresponding to M_1 , (3.19.2), is solved. The boundary conditions (3.17) are adjusted through shooting on w . Finally, the system with M , (3.19.3) is solved, and the boundary conditions (3.18) are adjusted through shooting on v_r^1 . We omit the details.

4.1 General properties of the flow. Typical solutions are illustrated below. Note that the parameters a , ρ and g are all set equal to 1 throughout. Tolerance parameters have been set equal to 10^{-10} for both the ODEs and the nonlinear solvers.

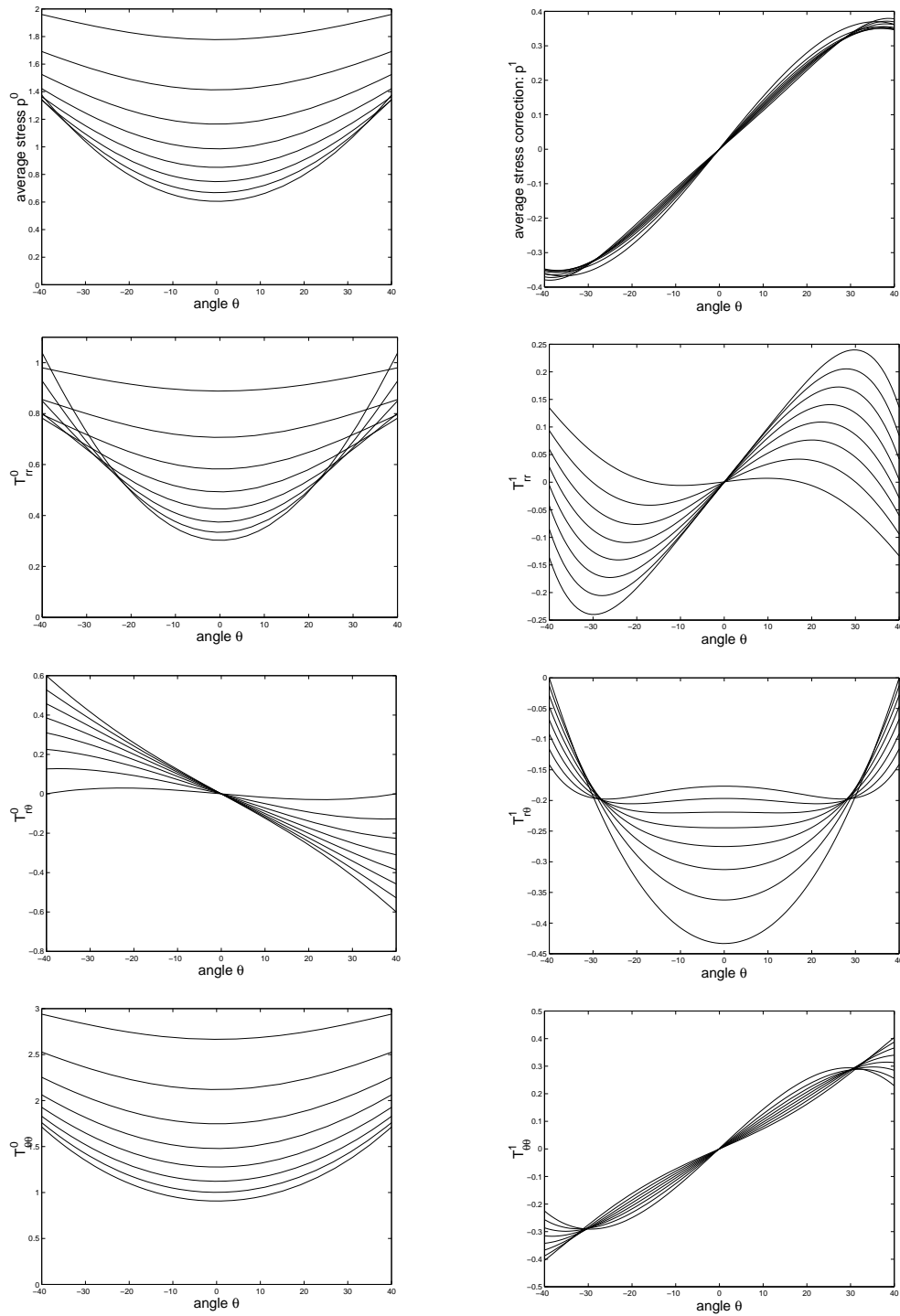


FIGURE 4.1. *Stress components of the problem with conical insert: angle of friction $\delta = 30^\circ$, half opening angle $= 40^\circ$ and wall friction $\mu = i/20, i = 0, \dots, 7$. In all the pictures except $T^1_{r\theta}$, $\mu = 0$ corresponds to the flatter curve.*

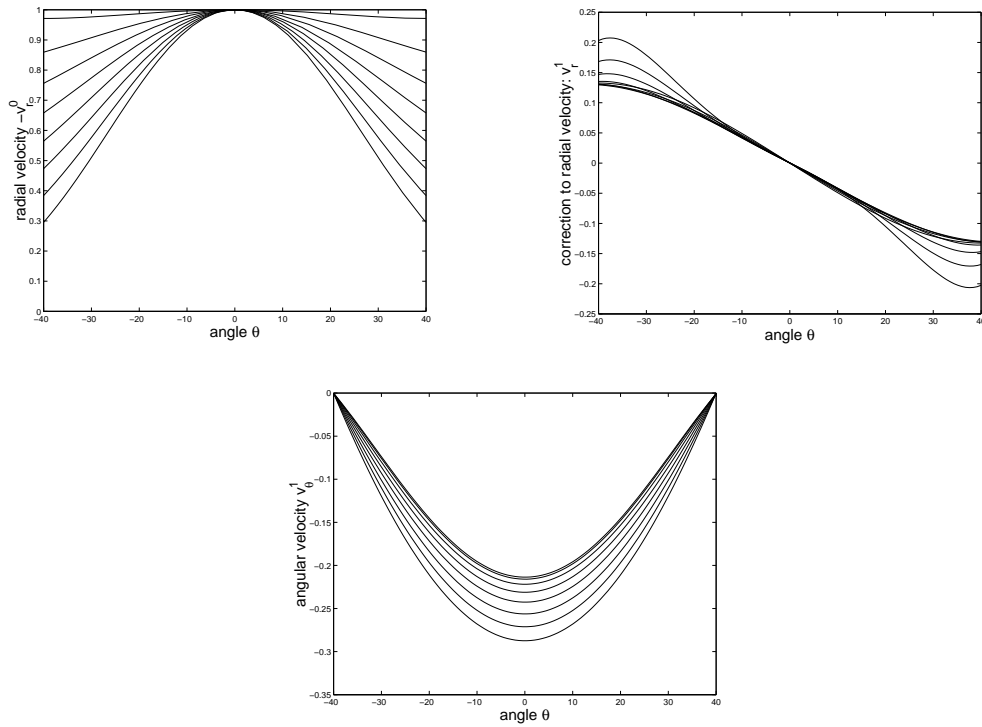


FIGURE 4.2. Velocity components of the problem with conical insert: angle of friction $\delta = 30^\circ$, half opening angle = 40° and wall friction $\mu = i/20, i = 0, \dots, 7$. In the first two pictures pictures, $\mu = 0$ corresponds to the flatter curve; the order is reversed for v_θ^1 .

Note that the above velocity fields have been normalized. The departure from a purely radial structure is visible by inspection of Figure 4.1 and 4.2. The behavior of the flow can also be illustrated by a look at the streamlines corresponding to the full velocity field (zero-th and first order).

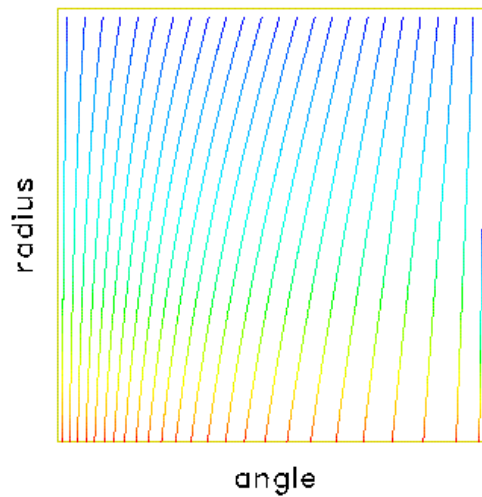


FIGURE 4.3. Streamlines from the velocity field.

4.2 Determination of the stagnant part of the flow. As noted at the end of Section 3, the problem becomes singular when

$$\psi_0 = \min\left\{\frac{\arccos(-\sin \delta)}{2}, \frac{\pi}{4}\right\} = \frac{\pi}{4}.$$

The first condition, in the middle term, corresponds to the stress equations, while the second is related to the velocity equations. Therefore, the velocity equations become singular “before” the stress equations. In other words, we can solve the M_0 -system, corresponding to the zero-th order stress terms and determine where the 0-th order velocity equation becomes singular. Following [7], we *interpret* the part of the flow beyond the point where the velocity field becomes singular as corresponding to the *stagnant* portion of the flow. This way, a “partial map” of the failure mode of the insert strategy is obtained. The present analysis implicitly assumes the stagnant zone to be radial, which is rarely the case in practice. The position of the critical ray, if it exists, separating the moving and stagnant parts of the flow is measured in the coordinate system of Figure 1.1 by a critical angle ϑ^* .

In Figure 4.4, the width of the flowing part is reported for a hopper with a 30° half opening angle, for various values of the angles of wall friction, $\Phi = \arctan(\mu)$, and internal friction δ .

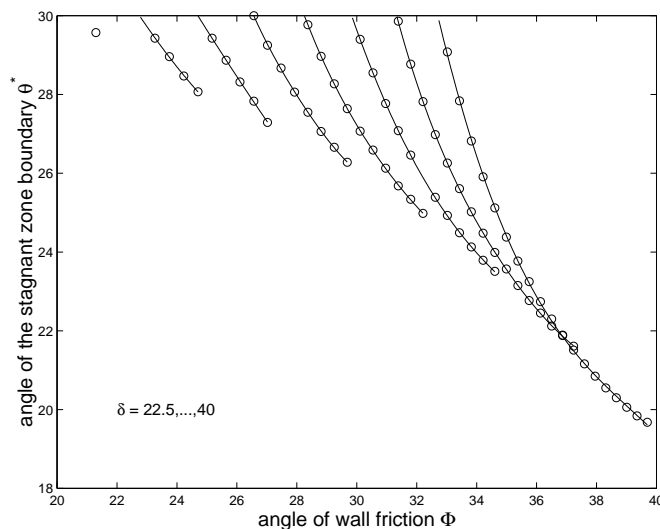


FIGURE 4.4. *Dependence of the stagnant zone boundary angle with angle of wall friction in a hopper with a 30° half angle for various values of the internal angle of friction δ between 22.5° and 40° .*

In Figure 4.4, a value of 30° corresponds to no stagnant zone. For values of δ smaller than those considered here, no stagnant zone was predicted. One observes that for each considered value of the internal angle of friction δ , there is a critical value of the wall friction, under which there is no stagnant region, and over which such an area appears. This critical value increases with δ . Further, for a fixed δ , the width of the stagnant part of the flow increases with the wall friction. On each curve, the lowest point corresponds approximately to values of the parameters at which the stress equations become singular, see (3.20).

4.3 Analysis of the insert's influence. The analysis is based on the characteristic curves. In order to construct the velocity characteristics, we go back to the original PDEs, and rewrite (2.10) and (2.11) as follows

$$\mathbb{A} \partial_r \begin{pmatrix} v_r \\ v_\vartheta \end{pmatrix} + \frac{1}{r} \mathbb{B} \partial_\vartheta \begin{pmatrix} v_r \\ v_\vartheta \end{pmatrix} = \mathbb{G},$$

where

$$\mathbb{A} = \begin{pmatrix} 1 & 0 \\ 0 & 1/2 \end{pmatrix}, \quad \mathbb{B} = \begin{pmatrix} 0 & 1 \\ 1/2 & -T_{r\vartheta}/(T_{\vartheta\vartheta} - p) \end{pmatrix};$$

the expression of the matrix \mathbb{G} is not relevant here. The velocity characteristics are then

$$\frac{1}{r} \frac{dr}{d\vartheta} = \lambda_{1,2}$$

where $\lambda_{1,2}$ are the eigenvalues of the matrix $\mathbb{B}^{-1} \mathbb{A}$. Elementary calculations lead to

$$\frac{1}{r} \frac{dr}{d\vartheta} = \frac{T_{r\vartheta}}{T_{\vartheta\vartheta} - p} \pm \sqrt{\frac{T_{r\vartheta}^2}{(T_{\vartheta\vartheta} - p)^2} + 1} \quad \vartheta \in (\vartheta_1, \vartheta_2). \quad (4.4)$$

The above relation, expressed in terms of the Sokolovskii variables, becomes

$$\frac{1}{r} \frac{dr}{d\vartheta} = \mp \tan\left(\frac{\pi}{4} \pm \psi\right). \quad (4.5)$$

To find the stress characteristics, (2.6) and (2.7) are rewritten using again the Sokolovskii variables

$$\mathbb{C} \partial_r \begin{pmatrix} \sigma \\ \psi \end{pmatrix} + \frac{1}{r} \mathbb{D} \partial_\vartheta \begin{pmatrix} \sigma \\ \psi \end{pmatrix} = \mathbb{H},$$

where

$$\mathbb{C} = \begin{pmatrix} 1 - \sin \delta \cos 2\psi & 2\sigma \sin \delta \sin 2\psi \\ -\sin \delta \sin 2\psi & -2\sigma \sin \delta \cos 2\psi \end{pmatrix}, \quad \mathbb{D} = \begin{pmatrix} -\sin \delta \sin 2\psi & -2\sigma \sin \delta \cos 2\psi \\ 1 + \sin \delta \cos 2\psi & -2\sigma \sin \delta \sin 2\psi \end{pmatrix};$$

\mathbb{H} is irrelevant here. The stress characteristics are then

$$\frac{1}{r} \frac{dr}{d\vartheta} = \mu_{1,2}$$

where $\mu_{1,2}$ are the eigenvalues of the matrix $\mathbb{D}^{-1} \mathbb{C}$. Note that \mathbb{D} is nonsingular as long as $\sin \delta + \cos 2\psi \neq 0$, which corresponds again to (3.20). One finds

$$\frac{1}{r} \frac{dr}{d\vartheta} = \mp \tan\left(\frac{\pi}{4} - \frac{\delta}{2} \pm \psi\right). \quad (4.6)$$

Incidentally, we observe from (4.5) and (4.6) that the velocity and stress characteristics are respectively at angles $\pm\pi/4$ and $\pm(\pi/4 - \delta/2)$ from the major principal stress. Numerically, the zero-th and first order velocity characteristics are constructed by solving (4.4) in conjunction with (3.15), where the stress components appearing in (4.4) are respectively taken at order zero and one. The stress characteristics are obtained by solving (4.6) in conjunction with (3.15), where $\psi = \frac{1}{2} \arctan\left(\frac{2T_{r\vartheta}}{T_{rr} - T_{\vartheta\vartheta}}\right)$, and with the stress components being again taken at order zero and one respectively. As a way of illustration, the downstream characteristic curves emanating from the top of the hopper are plotted in Figure 4.5.

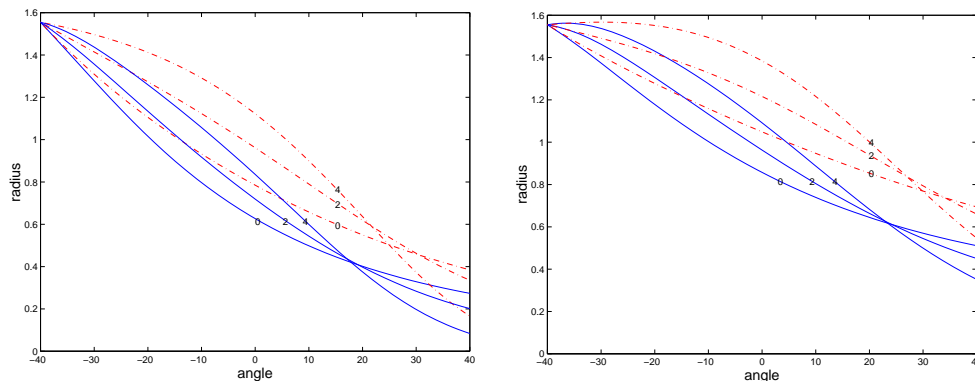


FIGURE 4.5. Left: zero-th (dashdot) and first order (solid) downstream velocity characteristics from the top of the insert; right: same curves for the stress characteristics. In both cases, the parameters are: angle of friction $\delta = 30^\circ$, half opening angle = 40° . The curves indexed 0, 2, 4 correspond to wall friction values of $\mu = 0, .2, .4$, respectively.

It is observed from Figure 4.5, that in neither case can the first order corrections be ignored.

We now turn to the main application of our method: the determination of “optimal” conical inserts, according to the criterion discussed in the Introduction. Following Johanson [5], we work with the stress characteristics. Numerically, the downstream stress characteristic curve emanating from the top of the hopper is first computed. Its intersection with the outer wall of the hopper is recorded (see Figure 4.6). Then, by a shooting method, the distance r^* , measured along the line from the origin to the top of the conical insert (see again Figure 4.6) is sought. The critical value r^* is so that the upstream characteristic curve from the bottom of the insert intersects the downstream characteristic curve from the top of the insert exactly on the outer hopper wall.

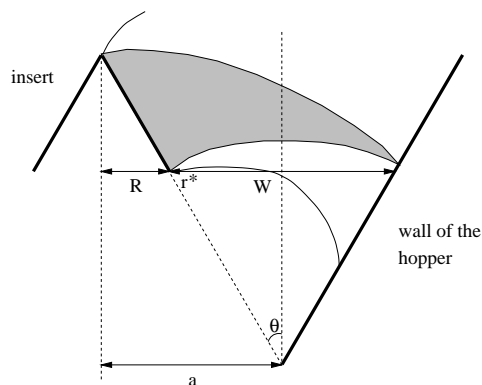


FIGURE 4.6. Geometry of the hopper/insert system.

In the calculations below, the results are expressed in terms of the dimensionless parameter W/R , where W is the horizontal distance between the bottom of the insert of the wall of the hopper, while R stands for the radius of the insert, see Figure 4.6. Equivalently, we have $W/R = 2r^* \sin \theta_W / (a - r^* \sin \theta_W)$, where the parameter a has been fixed equal to 1, and θ_W stands the half opening angle. The relationship between the opening angle, the internal friction and the optimal size of the insert is investigated

in Figure 4.7. The dependency of W/R on the wall friction is illustrated in Figure 4.8.

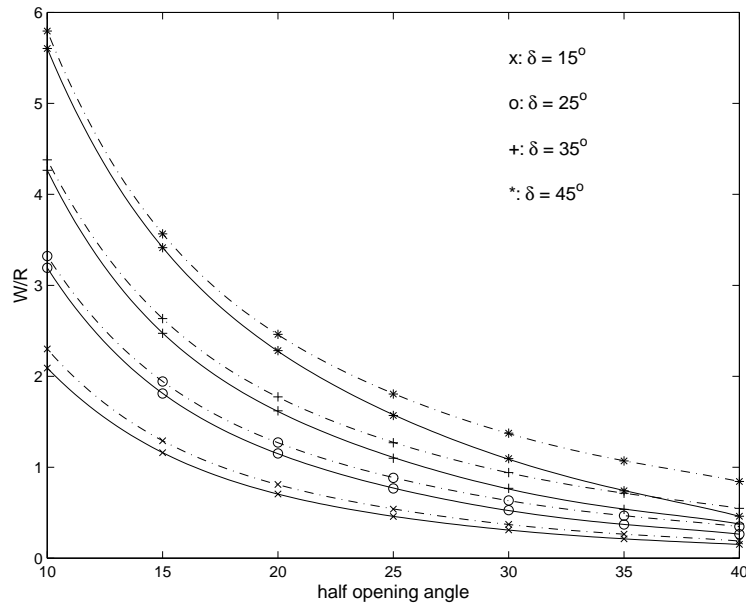


FIGURE 4.7. Approximate critical size of the hopper/insert system based on the stress characteristics; critical value W/R against the half opening angle, dashdot line: without correction, solid line: with correction. Wall friction $\mu = .2$.

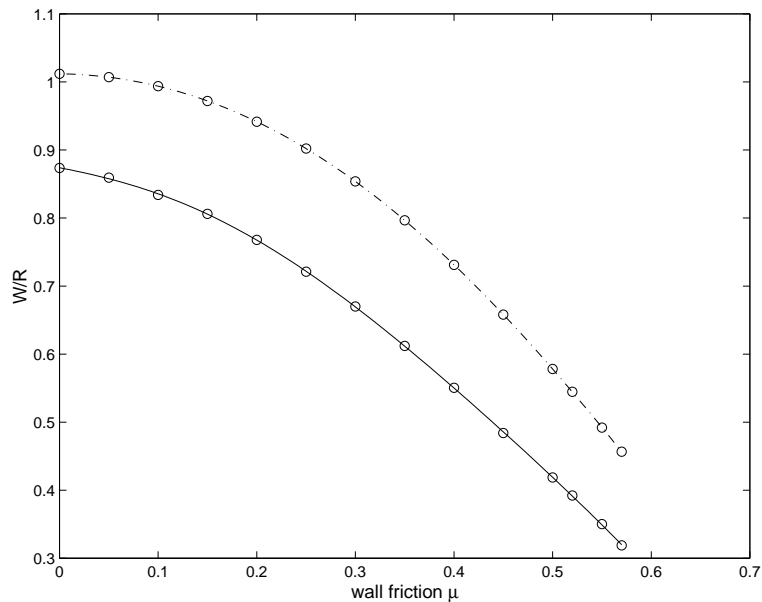


FIGURE 4.8. Approximate critical size of the hopper/insert system based on the stress characteristics; critical value W/R against the wall friction μ , dashdot line: without correction, solid line: with correction. Half opening angle 30° .

It is observed that for a fixed angle of internal friction δ and a fixed wall friction μ ,

W/R decreases as the opening angle increases, as expected. Further, the values of W/R computed through our analysis with first order correction are in every case between 4% and 30% smaller than those obtained without correction. This corresponds to requiring larger inserts. In other words, our criterion is somewhat more stringent than Johanson's. The difference between the two approaches is quite significant for large opening angles ($\approx 40^\circ$) and large angles of internal friction δ ($\delta \approx 45^\circ$), where it can reach 30% or more. Also, we note that our results at order zero, i.e., without correction, appear to be quite consistent with Johanson's results [5]. For instance, for a hopper with a 35° opening angle and with material parameters $\delta = 40^\circ$ and $\mu = \arctan(23^\circ)$, all of those being "large" values, Johanson reports the experimental value $W/R = 0.6$, and a corresponding computed value of 0.6. Without correction, we obtain $W/R = .5962$, but with correction, the computed value of W/R falls to .3732.

The discrepancy could stem from several reasons. First, our analysis is based on the von Mises yield condition, rather than the simpler Coulomb yield condition corresponding to both Johanson's analysis and our approach without correction. Second, as explained in the Introduction, the stress and velocity fields are *not* radial. Even though our expansion looks promising in that respect, how fast and where (if anywhere!) it converges is not clear. In other words, additional terms in the expansion might be needed. It appears that the resolution of the full system (2.6–2.11) will shed some light on this point [1]. Finally, the present criterion for insert design can be, and has been, put in question [10]. Indeed, it is, for instance, remarkable that if the same analysis is carried out with *velocity* characteristics instead of stress characteristics, much bigger inserts are found to be required (factor 4 to 10). The results obtained this way do not appear to agree in any way with the experimental values.

5. Conclusions. We have introduced a new method for the numerical resolution of granular flows around obstacles under strong geometrical restrictions, namely in the case of conical hoppers with inverted conical inserts. The method stems from an earlier construction, due to Jenike [2], of radial similarity solutions. The present approach differs from it by allowing for a more general structure of the solutions, which do not have to be radial. Further, since it leads to a system of ordinary differential equations with boundary conditions, it is still much simpler than the numerical resolution of the full system of partial differential equations corresponding to the problem [refgm].

It is found that for small values of the physical parameters (opening angle, internal and wall frictions), the present method leads to results quite comparable to the purely radial approach of Jenike. Our corrections become important for larger values of those parameters, i.e., when there is a sensitive departure from a radial structure. The discrepancy between those two methods has been illustrated here by our study of "optimal sized" inserts. The criterion used for the determination of the inserts is based on the stress characteristics and, to the authors' knowledge, was originally proposed by Johanson [5]. We note that there does not seem to be other than empirical justifications of that criterion which, nevertheless, appears to be quite useful (and used!) in practice [3]. Some authors [10] have rejected part of the good behavior of Johanson's criterion as being purely incidental.

Our method in conjunction with Johanson's criterion leads to more stringent conditions on the inserts than a purely radial approach. We will address in future work, through simulation of the full system, the question of whether this reflects on the validity, or the lack thereof, of either our expansion or Johanson's criterion

Acknowledgments. The authors are grateful to Tony Royal and his colleagues

at Jenike & Johanson, Inc., for several stimulating discussions.

REFERENCES

- [1] P. A. GREMAUD, J. V. MATTHEWS, *Numerical simulation of granular flows in hoppers*, In preparation.
- [2] A. JENIKE, *Gravity flow of bulk solids*, Bulletin No. 108, Utah Eng. Expt. Station, University of Utah, Salt Lake City.
- [3] T. A. ROYAL, *Private Communication*, Jenike & Johanson, Inc..
- [4] J. R. JOHANSON, *Stress and velocity fields in the gravity flow of bulk solids*, J. Appl. Mech., 31 (1964), pp. 499–506.
- [5] J. R. JOHANSON, *The use of flow-corrective inserts in bins*, Transactions of the ASME (1966), pp. 224–230.
- [6] S.B.M. MOREEA AND R.M. NEDDERMAN, *Exact Stress and Velocity Distributions in a Cohesionless Material Discharging from a Conical Hopper*, Chem. Eng. Sc., 51 (1996), pp. 3931–3942.
- [7] R.M. NEDDERMAN, *Statics and Kinematics of Granular Materials*, Cambridge University Press, 1992.
- [8] E. B. PITMAN, *The stability of granular flow in converging hoppers*, SIAM J. Appl. Math., 48 (1988), pp. 1033–1052.
- [9] D. G. SCHAEFFER, *Instability in the evolution equations describing incompressible granular flow*, J. Diff. Eqs., 66 (1987), pp. 19–50.
- [10] U. TÜZÜN AND R. M. NEDDERMAN, *Gravity flow of granular materials round obstacles-I: investigation of the effects of inserts on flow patterns inside a silo*, Chem. Eng. Sc., 40 (1985), pp. 325–336.

Appendix. The coefficients of the system (3.15) are as follows

$$\begin{aligned}
 A &= -\sin \delta \sin 2\psi^0, \\
 B &= -2\sigma^0 \sin \delta \cos 2\psi^0, \\
 C &= 1 + \sin \delta \cos 2\psi^0, \\
 D &= -2\sigma^0 \sin \delta \sin 2\psi^0, \\
 E &= \sin \delta, \\
 F &= -\frac{\sin^2 \delta}{2a} \sin \vartheta \cos 2\psi^0, \\
 G &= -2u \sin 2\psi^0 + 2v \cos 2\psi^0 + \frac{\sin^2 \delta}{a} \sigma^0 \sin \vartheta \sin 2\psi^0, \\
 H &= \cos 2\psi^0 + \sin \delta, \\
 I &= \sin 2\psi^0, \\
 J &= 2 \tan 2\psi^0, \\
 K &= \sigma^0 (1 - 3 \sin \delta \cos 2\psi^0), \\
 L &= -3\sigma^0 \sin \delta \sin 2\psi^0, \\
 M &= u(4 \sin \delta - 2 \cos 2\psi^0) - 2v \sin 2\psi^0 + \frac{\sigma^0}{a} \sin^2 \delta \left(\sin(\vartheta + 2\psi^0) + \sin \vartheta \cos 2\psi^0 \right), \\
 N &= -\frac{\sin^2 \delta}{2a} \sigma^0 \cos \vartheta \cos 2\psi^0 - 4v \sin \delta + \frac{\sigma^0}{a} \sin^2 \delta \cos(\vartheta + 2\psi^0), \\
 O &= 2 \tan 2\psi^0 v_r^0, \\
 P &= 2 \tan 2\psi^0 v_r^1 - v_\vartheta^1 + \frac{\sin 2\psi^0}{\sigma^0 \sin \delta \cos^2 2\psi^0} \left(2u + \frac{\sin \vartheta}{a} \sigma^0 \sin \delta \cos 2\psi^0 \right) v_r^0, \\
 Q &= v_r^1 + \frac{\sin \vartheta}{a} v_r^0.
 \end{aligned}$$

The relations between the variables of (3.15) of the physical components of the stress are follows

$$\begin{aligned}
T_{rr}^0 &= \sigma^0 (1 - \sin \delta \cos 2\psi^0), & T_{rr}^1 &= \sigma^1 - u, \\
T_{r\vartheta}^0 &= -\sigma^0 \sin \delta \sin 2\psi^0, & T_{r\vartheta}^1 &= -v, \\
T_{\vartheta\vartheta}^0 &= \sigma^0 (1 + \sin \delta \cos 2\psi^0), & T_{\vartheta\vartheta}^1 &= \sigma^1 + u, \\
T_{\varphi\varphi}^0 &= \sigma^0, & T_{\varphi\varphi}^1 &= \sigma^1 + \frac{\sin \vartheta}{3a} \sigma^0 \sin \delta \cos 2\psi^0,
\end{aligned}$$

where $\sigma^1 = \frac{1}{\sin \delta} \left(u \cos 2\psi^0 + v \sin 2\psi^0 - \frac{\sin^2 \delta}{2a} \sigma^0 \sin \vartheta \cos 2\psi^0 \right)$.